On the Role of Eddy Mixing in the Subtropical Ocean Circulation

Tongya Liu[1], Hsien-Wang Ou[2], Xiaohui Liu[1,3], and Dake Chen[1,3]

[1] State Key Laboratory of Satellite Ocean Environment Dynamics, Second Institute of Oceanography, Ministry of Natural Resources, Hangzhou, Zhejiang, China.

[2] Lamont-Doherty Earth Observatory, Columbia University, New York, NY, USA (Retired).

[3] Southern Marine Science and Engineering Guangdong Laboratory (Zhuhai), Zhuhai, China.

Corresponding author: Dake Chen (dchen@sio.org.cn)

Key Points:

- Four horizontal resolutions are used to compare the structure of the upper-ocean circulation
- From 1° to 1/32°, the eddy mixing reduces the latitudinal PV range to about 25%
- Sverdrup relationship should be treated carefully in the eddy-rich region, even in the subtropical interior

Abstract

Most of the classic wind-driven circulation theories based on the Sverdrup balance have neglected the profound influence of eddy mixing on the large-scale distribution of the potential vorticity (PV), thus failing to explain some prominent features of the observed circulation. In this study, using a series of numerical experiments based on the MITgcm, we diagnose the PV balance to quantify the effect of eddy mixing on the subtropical gyre. Four grid-spacings of 1, 1/3.2, 1/10, and 1/32 degrees are selected to compare the structure of the upper-ocean circulation. In the 1° grid case, the structure of the thermocline is as predicted by the Sverdrup dynamics, with its maximum depth located in the subtropical interior where the wind stress curl is strongest. With increasing resolution, however, this maximum depth is displaced toward the subtropical front, which more closely resembles the observed thermocline. From 1° to 1/32°, the enhanced eddy mixing tends to homogenize the macroscopic PV in the subtropical gyre and reduces the latitudinal PV range to about 25% of the non-eddy solution; and the region where the Sverdrup balance holds is relegated to isolated patches, with its area reduced by about 60%. Furthermore, sensitivity experiments show that the observed thermocline structure is well reproduced in eddy-resolving runs, indicating that the PV mixing provides a better explanation of the subtropical circulation than the Sverdrup dynamics. Our results suggest that the Sverdrup relationship should be treated carefully in the eddy-rich region, even in the subtropical interior.

Keywords: eddy mixing; MITgcm; potential vorticity homogenization; Sverdrup balance; subtropical gyre

Plain Language Summary

The subtropical ocean gyre is a great conveyor for water, heat, and material, and is playing a key role in the global climate system. The traditional theories suggest the subtropical gyre is driven by wind and satisfied with a simple Sverdrup balance. However, these classical theories are seriously challenged by new observational evidence and discoveries because they fail to describe some observed features of the upper ocean circulation, which might be attributed to neglecting the effects of oceanic eddies. In this manuscript, we conduct a series of numerical experiments with four different horizontal resolutions ranging from 1 degree to 1/32 degree and compare the structure of the upper-ocean circulation. Our simulations show that the enhanced eddy mixing effectively homogenizes the potential vorticity field in the subtropical gyre and significantly degenerates the standard Sverdrup balance. And sensitivity experiments indicate that the subtropical circulation is better described by the eddy mixing regime than the traditional dynamics. These results present a profound change to our understanding of the classic circulation theory and the effects of eddy mixing are essential in a more complete large-scale ocean circulation theory.

1 Introduction

With the advent of satellite observation over the past few decades, our knowledge of the structure and variability of the upper ocean circulation has improved significantly. The ubiquitous occurrence of eddies has been considered as the most prominent feature in the upper ocean (Fu et al. 2010). The motion with horizontal scales of 1-100 km (submeso- to meso-scale) would cause strong mixing of macroscopic fields that are materially conservative, such as temperature and potential vorticity (PV), which are closely linked with the structure of the general ocean circulation (e.g., Lévy et al. 2010; Marshall et al. 2002; Su et al. 2018; Wenegrat et al. 2018).

Classical wind-driven circulation theories based on an interior Sverdrup (1947) balance have been widely accepted since their formulation. Considering a homogeneous ocean, a series of papers have produced the western-intensified subtropical circulation when subjected to bottom friction (Stommel 1948), lateral friction (Munk 1950), and inertial boundary layer (Charney 1955). Subsequently, multilayer models with ventilated thermocline are proposed and developed by Luyten et al. (1983) and Huang (1988) to examine the flows in the subtropical interior. Besides, inertial models of ocean gyres are introduced by Fofonoff (1954) and the barolinic extension is explored by Marshall and Nurser (1986) based on the quasi-geostrophic formulation. However, even a Sverdrup interior is now seriously challenged by recent observational evidence and analysis. On the one hand, the predictions based on the Sverdrup dynamics are at odds with some salient features observed. Stommel (1965, Chapter 8) notes that the thermocline deepens linearly with the latitude in the subtropical gyre, rendering the columnar PV above the thermocline nearly constant. A similar feature is also noticed by Qiu et al. (2010) from multi-year repeated observations in the North Pacific. On the other hand, the Sverdrup balance neglects the effect of eddy mixing on the PV distribution. The prevalence of eddies has changed our conception of ocean currents from quasi-steady to highly variable since the eddy kinetic energy (EKE) is about two orders of magnitude greater than the mean kinetic energy (Munk, 2002).

The effect of strong eddy mixing on the subtropical circulation has been explored in many numerical studies. Rhines and Young (1982) demonstrate via a quasi-geostrophic model that the weak eddy mixing can drive subsurface flow and homogenizes the PV field in closed gyres. Cox (1985) compares coarse-grid (1°) and fine-grid (1/3°) solutions from a 3D primitive equation model and shows that eddy mixing tends to homogenize the PV along isopycnals in the subtropical gyre. Using diagnostics of transformed Eulerian mean, Henning and Vallis (2004) demonstrate that eddies can move the density outcrop and modify the shape of the main thermocline in an eddy-permitting (1/6°) model. Their results are re-examined by Lévy et al. (2010) at a higher resolution (1/54°), which further highlights the significant role of the submesoscale processes in the mean circulation. Besides, Hogg and Gayen (2020) represent that the subtropical and subpolar gyres could be reproduced without wind in an eddy-permitting basin.

As a step in his formulation of a climate theory based on the nonequilibrium thermodynamics that fully accounts for the eddy mixing, Ou (2013) derives the general atmospheric circulation within the thermodynamical closure. The troposphere is reduced by eddy mixing to tropical and polar air masses within which the PV is homogenized, a configuration that is supported by observational analysis. Since the resulting upper-bound wind resembles the prevailing wind, it supports the PV homogenization as a viable dynamical principle in explaining the general atmospheric circulation. Given the strong eddy activity in the ocean and the homogenized PV observed in the subtropical gyre (Stommel 1965; McDowell 1982; Talley 1988), we apply the same principle of PV homogenization by eddy mixing to explain the general ocean circulation (see Section 4).

Previous studies (e.g., Cox 1985; Smith et al. 2000; Henning and Vallis 2004; Lévy et al. 2010) have examined the effect of eddy mixing in the subtropical gyre, but the effect on the PV homogenization has yet to be quantified. In addition, the relative importance of the Sverdrup dynamics and PV mixing in the upper ocean circulation remains unclear. In this study, we aim to investigate the role of eddy mixing in the subtropical circulation by diagnosing the PV balance. Particularly, we wish to explore the following issues: (1) the extent to which the eddy mixing homogenizes the PV field and affects the dynamical structure of the subtropical gyre; (2) a quantitative comparison of the two different regimes of Sverdrup dynamics and PV homogenization.

2 Numerical model

In this study, the MITgcm (Marshall et al. 1997) is used to calculate the subtropical circulation. As in Cox (1985), we consider a rectangular basin spanning 60° in both longitude and latitude, bounded to the south by the equator. The basin has a uniform depth of 4000 m with a narrow sloping wall along its western boundary (the depth increases exponentially from 200 to 4000 m in 4°). Unlike Cox (1985), we use a straight western boundary to avoid unnecessary complication of the topographic effect. The vertical z-coordinate has 29 levels with grid spacing increasing from 10 m at the surface to 500 m at depth, as used by Liu et al. (2019) in their simulation of the teeming eddies.

The linear equation of state is adopted in the model. Setting salinity at 35 PSU, the density is linked to the temperature via

$$\rho = \rho_{\mathrm{ref}} + 1000[-\alpha_{\mathrm{T}}(\mathrm{T} - 20)], \tag{1}$$

where the reference density ρ_{ref} is set at $1025\ \mathrm{kg \cdot m^{-3}}$ and the thermal expansion coefficient α_{T} is set to $2 \times 10^{-4}\ ℃^{-1}$. The model is driven by zonally uniform wind stress that is shown in Figure 1(a). Three wind profiles, corresponding to weak, medium, and strong wind stress curl in the subtropical gyre, are used in the experiments, and the latitude of maximum wind stress curl is around 24°N. To simulate the differential surface heating, the surface density is restored to $\rho^* = \sigma_{\mathrm{T}} + 1000$, where σ_{T} is given by

$$\sigma_T = \begin{cases} 23 + 3y/36, & y \le 36°\mathrm{N} \\ 27 + (y - 36)/24, & 36°\mathrm{N} < y \le 60°\mathrm{N} \end{cases}. \tag{2}$$

The restoration time scale for the surface density is taken to be 40 days (for the top layer of 10 m), which implies a restoration coefficient $\gamma = 0.25\ \mathrm{m \cdot day^{-1}}$. A density "jump" at 36°N aligning with the maximum eastward wind is imposed to simulate the deep convection just poleward of the subtropical front (McCartney and Talley 1982).

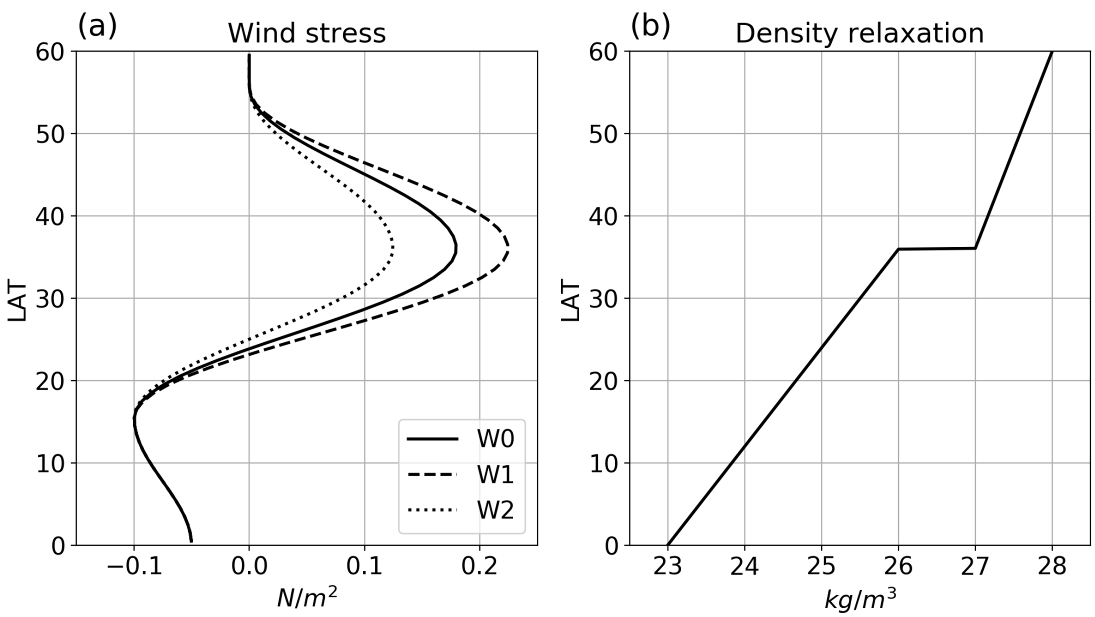

Figure 1. Surface forcing of the model. (a) Zonal wind profiles. The solid line (W0) is the zonal wind used in experiments D1, D3.2, D10, and D32. The other two lines are the zonal wind used in sensitivity experiments. (b) Restoring sea surface density. A density "jump" at 36°N is specified to simulate the strong convective overturning poleward of the subtropical front, as in the real ocean.

To assess the role of eddies, four horizontal grid spacings of 1°, 1/3.2° 1/10°, and 1/32° are used, which will be referred to as coarse-grid, eddy-permitting, eddy-resolving, and fine-grid, and designated by D1, D3.2, D10, and D32 experiments ("D" for "Degree"), respectively. To our knowledge, 1/10° grid has often been referred to as “high resolution” in the past two decades until more “super-high resolution” numerical calculations are carried out recently, such as 1/48° by Rocha et al. (2016) and 1/64° by Hurlburt and Hogan (2000). These studies however concern mainly with simulating the eddies while our aim is to assess the eddy effect on the mean circulation, which turns out to be adequately addressed by the range of the grid spacings we have selected. There is no need for us to pursue excessively on the reduction of the grid spacing.

All experiments with varying resolutions and wind profiles are summarized in Table 1. Experiments D1, D3.2, D10, and D32 are driven by the same wind profile (W0) and the experiments using wind profiles W1 and W2 are tagged as D1W1 and D1W2, D10W1 and D10W2 correspondingly. They are compared with D1 and D10 to examine the model sensitivity to the wind forcing. The model integrations are carried out in two stages of spin-up and experimental run. First, the 1° model is initialized from rest with vertical stratification derived from the World Ocean Atlas 2013 uniformly applied to the whole basin, and integrated for 250 years to reach a quasi-equilibrium. From this point on, all experiments are run for another 50 years, which is found sufficient to equilibrate the main thermocline (not shown). The time-average over the last 20 years is used for the following analysis.

For the 1° case, horizontal dissipation is provided by a Laplacian viscosity ($\mathrm{A_h} = 1 \times 10^4\ \mathrm{m^2 \cdot s^{-1}}$). For the other cases, the biharmonic viscosity by the modified Leith scheme (Fox-Kemper and Menemenlis 2008) is used. In addition, the vertical viscosity is set to $1 \times 10^{-4}\ \mathrm{m^2 \cdot s^{-1}}$, and the diapycnal diffusivity is $1 \times 10^{-7}\ \mathrm{m^2 \cdot s^{-1}}$. Further details of the physical parameters used in the model are available at https://github.com/liutongya/PV_circulation.

Table 1. Experiment designation.

Experiment ID	Resolution	Wind profile
D1	1°	W0
D3.2	1/3.2°	W0
D10	1/10°	W0
D32	1/32°	W0
D1W1	1°	W1
D10W1	1/10°	W1
D1W2	1°	W2
D10W2	1/10°	W2

3 The structure of the upper ocean circulation

It is expected that higher resolution models contain more energetic eddies and simulate the finer structure of the upper ocean (Bryan et al. 2007; Levy et al. 2010; Chassignet and Xu 2017). Figure 2 shows random snapshots of the sea surface temperature in D1, D3.2, D10, and D32. It is seen that the coarse-grid experiment (D1) cannot resolve mesoscale eddies, and the eddy-permitting experiment (D3.2) can reveal the temperature disturbance induced by large-size eddies. In the eddy-resolving experiment (D10), the basin is full of mesoscale eddies, especially in the subtropical gyre (between 10°N and 40°N). The fine-grid experiment (D32), in addition to mesoscale eddies, also resolves submesoscale and filamentary structures resulting from nonlinear processes; the ensuing chaotic advection is known to be particularly effective in mixing the macroscopic field (Brown and Smith 1991). Figure 3 shows zonally-averaged eddy kinetic energy (EKE) at the surface. The EKE of D1 is near zero, so the mean flow represents the instantaneous field. For the other experiments, the EKE varies with the latitude and all peak just south of the subtropical front. In D10, the maximum EKE exceeds $1000\ \mathrm{cm}^2 \cdot \mathrm{s}^{-2}$ and in D32, it is further doubled to $2000\ \mathrm{cm}^2 \cdot \mathrm{s}^{-2}$. As the latter is what observed from the AVISO-derived geostrophic currents (Renault et al. 2017), we surmise that the fine-grid experiment has adequately captured the effect of eddy mixing on the large-scale fields. We shall next diagnose this eddy effect on the upper-ocean circulation.

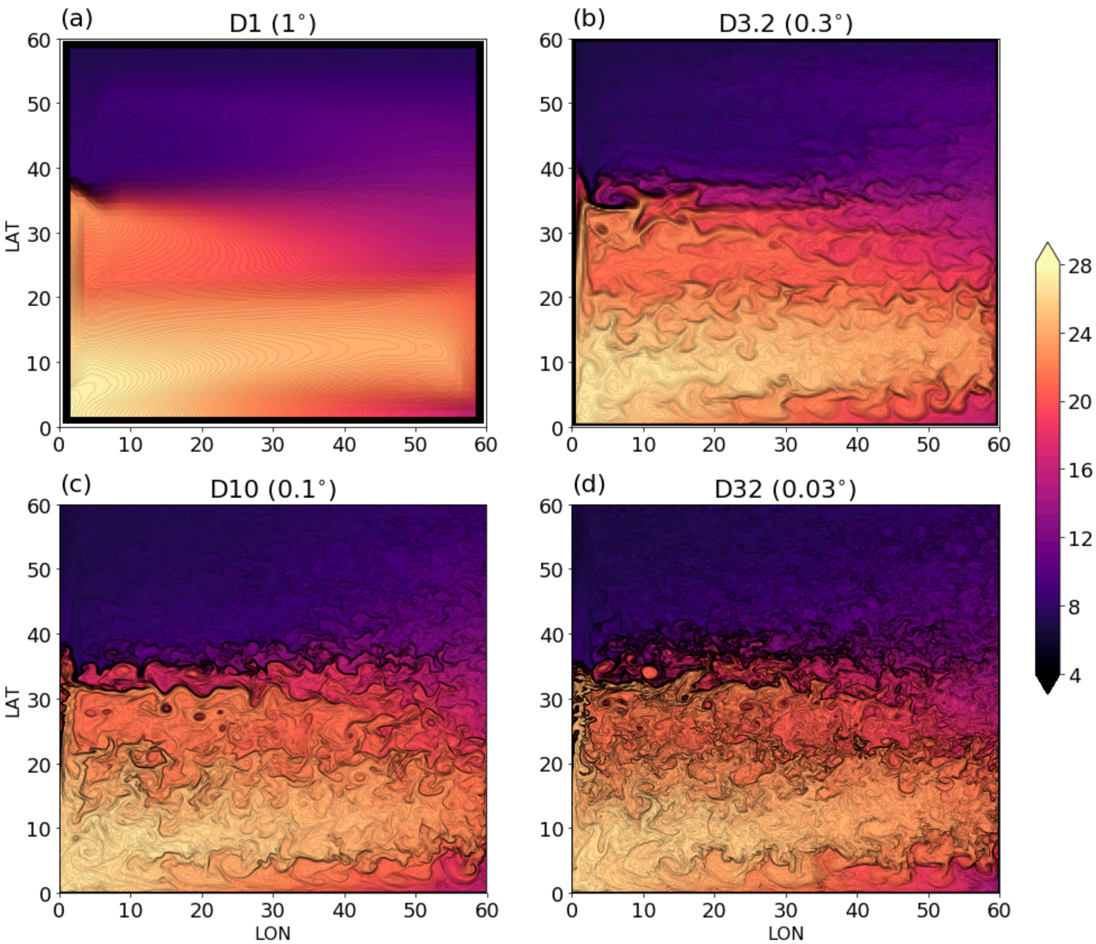

Figure 2. Snapshots of sea surface temperature (in °C) in experiments (a) D1, (b) D3.2, (c) D10, and (d) D32. Black contours of 0.1 °C interval are plotted to delineate the eddies.

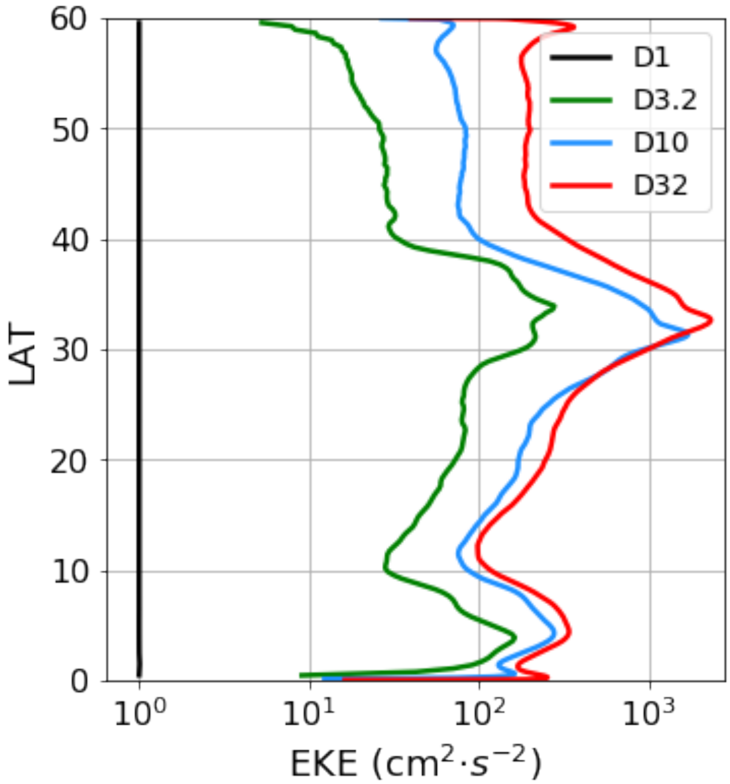

Figure 3. Zonal-averaged EKE (in $cm^2 \cdot s^{-2}$) at the surface from the four experiments.

Figure 4 shows the mean sea surface height (SSH) from the four experiments. In all cases, the zonal wind stress drives a classical double gyre (subtropical and subpolar) circulation pattern with a strong eastward current between the two gyres resembling the Gulf Stream extension (GSE) or Kuroshio extension (KE). On account of the hydrostatic balance, the depth of the main thermocline should reflect that of the SSH. According to the Sverdrup dynamics, this depth should respond to the Ekman pumping (Welander 1968), which is downward (upward) in the subtropical (subpolar) region. In D1, the latitude of the maximum thermocline depth roughly coincides with that of the maximum wind stress curl, as expected from the Sverdrup dynamics. The qualitative changes in the circulation pattern with increasing resolution however are significant. Compared with D1, the maximum depths of the thermocline in D10 and D32 are seen to move northward from the subtropical interior (about 24°N) to just south of the subtropical front (about 30°N). Moreover, their SSH patterns are quite comparable to the mean dynamic topography observed in the North Pacific or the North Atlantic (see Figure 3 in Rio et al. 2011).

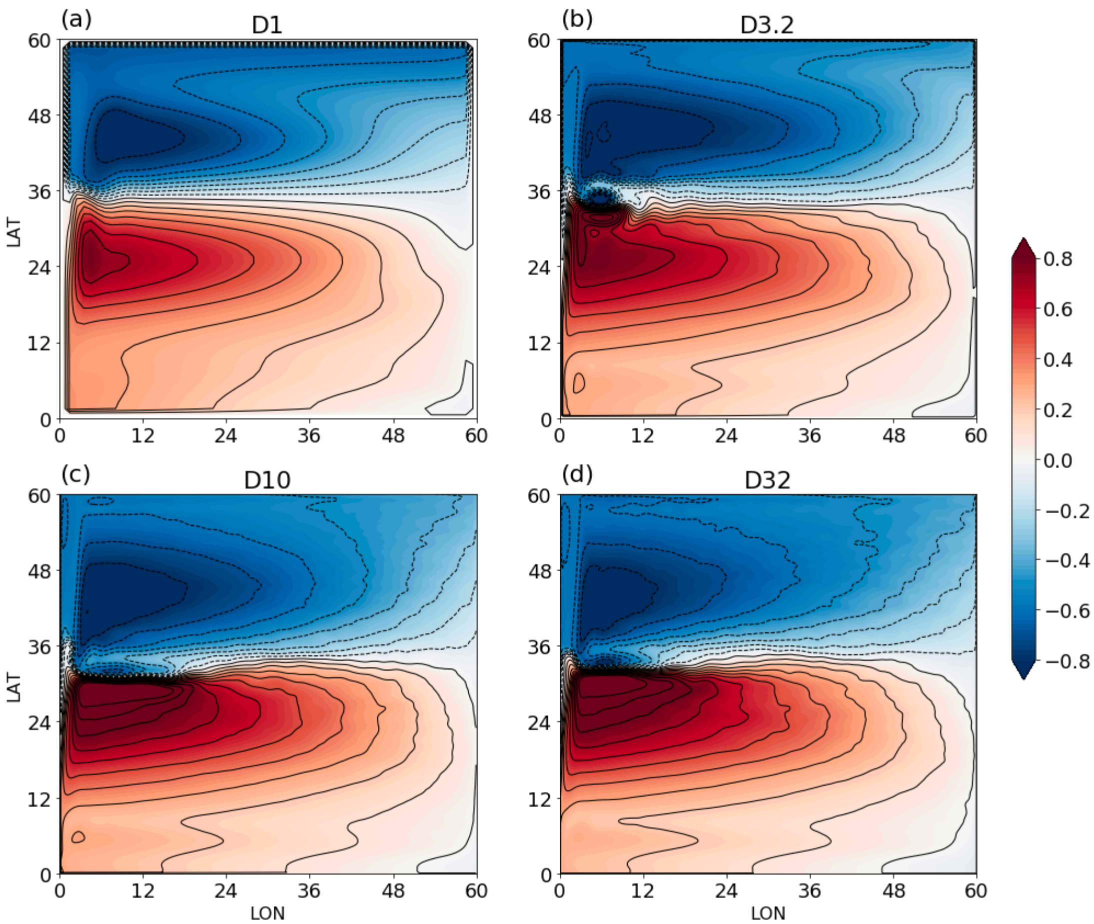

Figure 4. Time-averaged SSH (in meters) from the four experiments. The contour interval is 0.1 m.

To understand the differences in the flow structure among the four solutions and diagnose the eddy effect within the subtropical gyre, Figure 5 shows the spatial distribution of the EKE in D32. It is seen that the surface EKE is greater than $100\ \mathrm{cm}^2 \cdot \mathrm{s}^{-2}$ throughout the subtropical gyre, and exceeds $1600\ \mathrm{cm}^2 \cdot \mathrm{s}^{-2}$ near the subtropical front. In the vertical, the EKE is greater than

$100\ \mathrm{cm}^2 \cdot \mathrm{s}^{-2}$ above 400 m in the subtropical interior and above 800 m just south of the subtropical front. Compared with Cox (1985) and Henning et al. (2004), there is a significant improvement of the horizontal and vertical distribution of the EKE in our model, which should better capture the eddy effect on the mean temperature and PV fields.

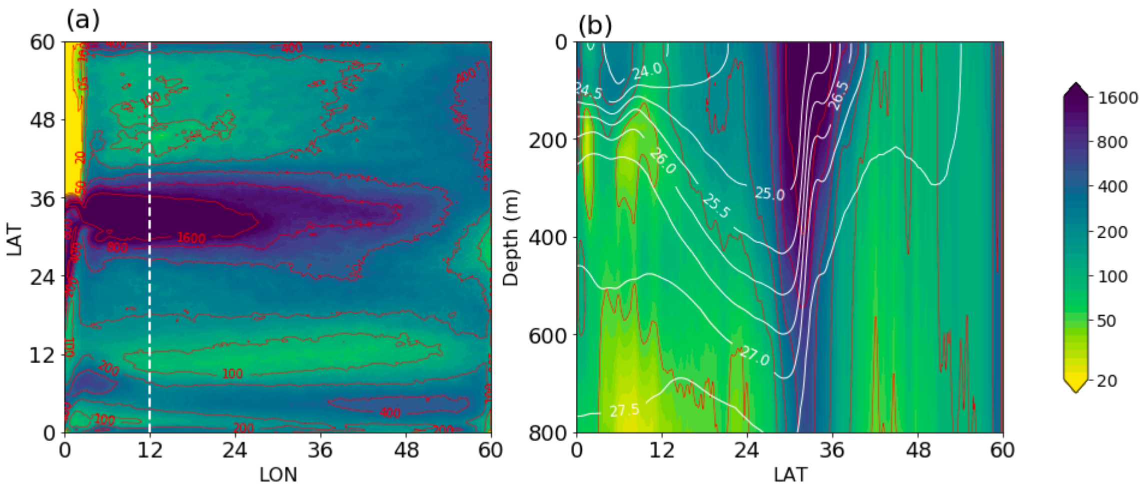

Figure 5. Spatial distribution of the EKE in D32. (a) The surface map; (b) The meridional section along 12°E, overlaid by the density field (white contours).

Figure 6 shows isopycnals and zonal velocity along the 12°E meridian with the isopycnal 26.5 (green line) marking the main thermocline. Our model has reproduced the main tropical and subtropical flows (Qiu et al. 2010), such as the westward North Equatorial Current (NEC), the eastward GSE, and the eastward Equatorial Undercurrent (EUC). Model solutions show significant improvement in the strength and width of these currents with increasing grid resolution. In D1, the NEC is comparable with the GSE in both width and speed, which is at odds with observations. In D3.2, the GSE becomes much more concentrated in a narrow latitudinal band and moves faster than that in D1. This trend continues for D10 and D32 when the GSE reaches speed exceeding 1 m/s, much closer to its observed speed (Hall 1989).

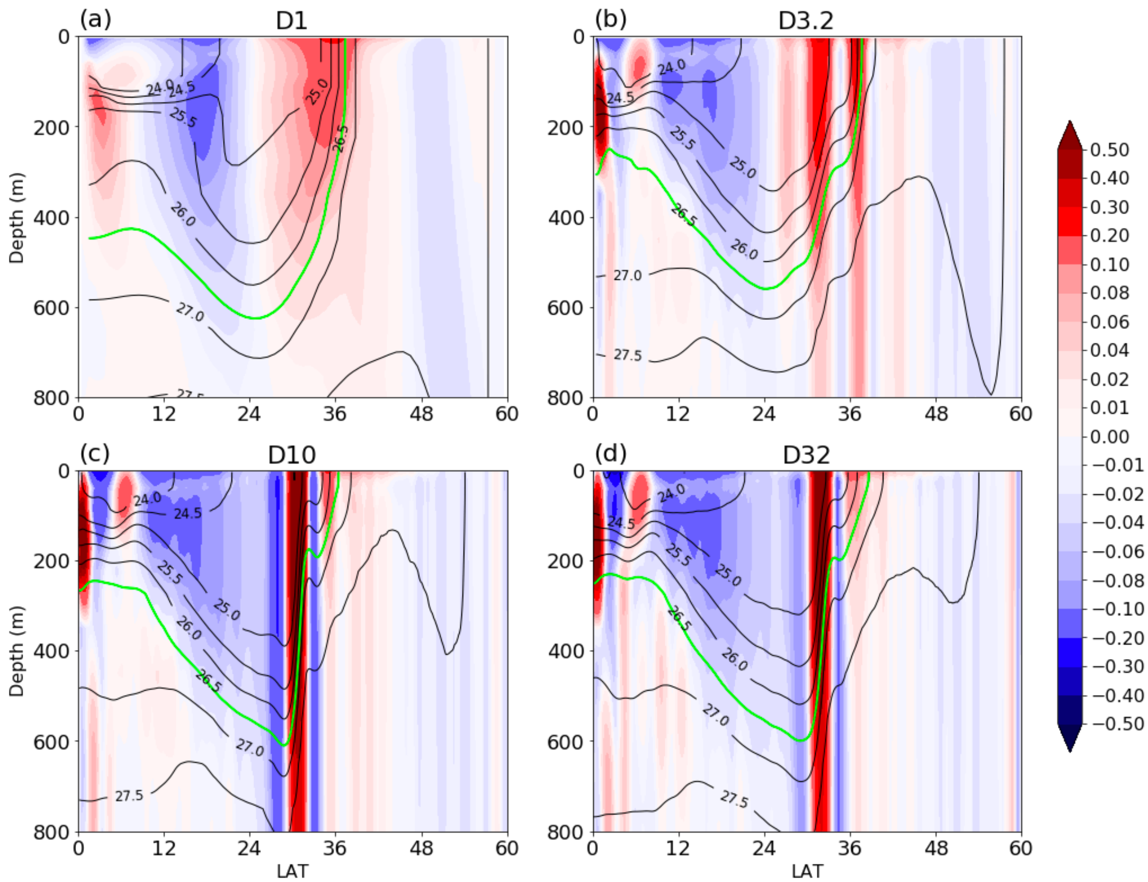

Figure 6. Meridional sections of zonal velocity (colored) and density (contoured) along 12°E, with the green line marking the main thermocline.

As discussed in connection with Figure 4, the increasing resolution also has profound effects on the thermocline shape. In D10 and D32, it is seen that the thermocline deepens linearly with the latitude from 10°N to about 30°N and then rises sharply across the GSE. This structure cannot be captured by the Sverdrup dynamics hence the coarse-grid experiment. That the thermocline in the subtropical gyre deepens linearly with the latitude was first noticed by Stommel (1965) from which he surmised that the columnar PV above the main thermocline should be homogenized. Previous numerical models have demonstrated that the GSE is narrower and stronger in the eddy-resolving runs, but they fail to reproduce the above thermocline structure, which we attribute to their insufficient grid resolution to fully capture the effect of strong eddy mixing (Henning et al. 2004).

4 PV homogenization in the subtropical gyre

Having described the circulation structure for four experiments, we now focus on the core issue of this study by diagnosing the PV balance. The key question is how the eddy mixing affects the PV distribution and upper-ocean circulation in the subtropics. For the columnar motion above the main thermocline, the macroscopic PV balance is described as (Young 1987; Ou 2013):

$$\vec{u} \cdot \nabla P - \nabla \cdot (k \nabla P) = \frac{1}{h} \hat{k} \cdot \nabla \times \frac{\vec{\tau}}{\rho_0 h}, \tag{3}$$

where

$$P = (f + \hat{k} \cdot \nabla \times \vec{u})/h \tag{4}$$

is the columnar PV, with f, the Coriolis parameter, h, the thermocline depth, $\vec{u} = (u, v)$, the horizontal velocity, $\vec{\tau} = (\tau^x, \tau^y)$, the wind stress, ρ_0, the reference ocean density, and k is the eddy diffusivity. Eq. (3) states that the PV input by wind (the RHS) is balanced by the mean advection (the first term) and eddy mixing (the second term). If the eddy mixing and the relative vorticity are neglected, the equation is reduced to the generalized Sverdrup balance above the thermocline (Welander 1968),

$$\beta h v = \hat{k} \cdot \nabla \times \frac{\vec{\tau}}{\rho_0}. \tag{5}$$

However, the Sverdrup balance would be nullified if the eddy mixing dominates the mean advection. In the asymptotic limit of large eddy diffusivity, Eq. (3) implies that the PV would be a harmonic function. Subjected to the Neuman condition of vanishing normal PV gradient (since the normal flux is finite to balance the wind input), the PV is then homogenized.

Maps of isopycnal PV (IPV) calculated from hydrographic data show a high degree of homogenization in the subtropical interior (Holland et al. 1984; Keffer 1985; Talley 1988), and the meridional section shows that IPV isolines are nearly parallel to the isopycnals between the tropics and the subtropical front (McDowell et al. 1982). Computationally, primitive-equation models (Cox 1985; Nakamura and Kagimoto 2006) show the PV homogenization in the upper layers where eddies are active. Our experiment D3.2 has reproduced the results of Cox (1985) that eddy mixing is quite effective in homogenizing IPV in the interior, and the experiment D32 shows even higher degree of the homogenization of the IPV (not shown). In this study, however, we focus on the columnar PV, rather than IPV, which can be directly translated to the subtropical gyre above the main thermocline --- the primary feature of the general ocean circulation that we are concerned with.

From the thermocline depth, we calculate the columnar PV based on Eq. (4), which is shown in Figure 7. It is seen that the PV distribution in D1 is as expected from the Sverdrup balance with strong gradients in the subtropical interior to reflect the PV input by the wind stress curl. In D3.2, the weak eddy mixing only marginally modifies the PV distribution between about 10°N and 25°N. In D10 and D32, however, the PV is seen to be significantly homogenized in the subtropical interior with its gradient expelled to the tropics, the western boundary and the subtropical front, which agrees with the observational analysis of Stommel (1965) and Toole et al. (1990). Our model thus has captured the effect of the eddy mixing of PV to render gyre-wide homogenization of the macroscopic PV. It is worth noting that although the EKE has doubled from D10 to D32, the homogenized area has not significantly expanded because it has already covered the full domain of the subtropical gyre. Since the subtropical gyre constitutes a primary feature of the upper ocean circulation, the PV homogenization, which spans the gyre, thus may provide the governing principle of the general ocean circulation.

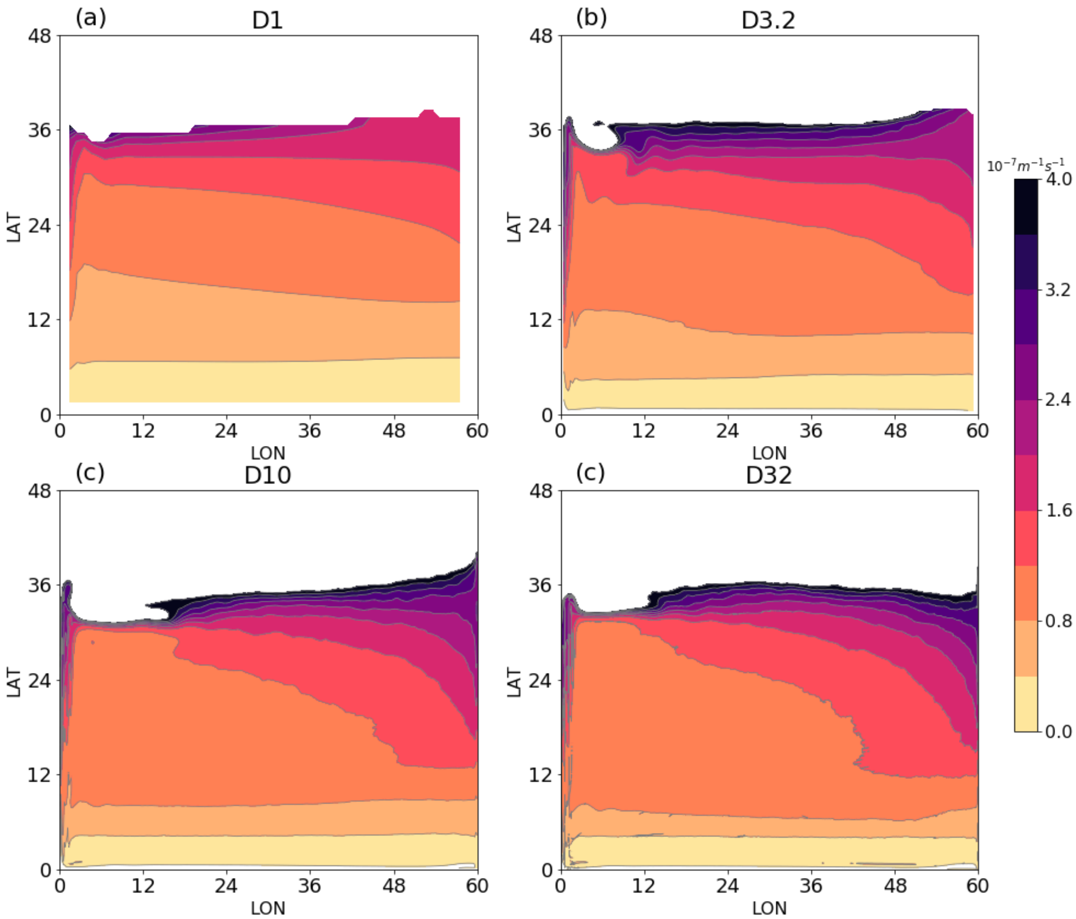

Figure 7. Time-averaged columnar PV (in $10^{-7}\ \mathrm{m}^{-1} \cdot \mathrm{s}^{-1}$) calculated from the thermocline depth.

Ou (2018) has generalized the thermohaline circulation (THC) from the coarse-grained meridional overturning cell to include random eddy exchange across the subtropical front. The strength of the THC (K) can be diagnosed from the buoyancy balance of the mode water

$$\int_0^l \gamma(\rho^* - \rho)dy = K\Delta\rho, \tag{6}$$

where ρ^* is the restoring surface density, γ is the restoration coefficient, l is the outcrop latitude, and $\Delta\rho$ is the density difference between the warm layer and the subpolar region. In the 1/32° run, the buoyancy gained by the warm layer south of the subtropical front (the LHS) is about $4.8\ \mathrm{kg}\cdot\mathrm{m}^{-1}\cdot\mathrm{s}^{-1}$, and $\Delta\rho$ has a range of $[0.75-1]\ \mathrm{kg}\cdot\mathrm{m}^{3}$, so K is calculated to be $[4.8-6.4]\ \mathrm{m}^{2}\cdot\mathrm{s}^{-1}$.

Since this same K transports the PV across the subtropical front, its diagnosis allows us to estimate the homogenized PV from the PV budget of the warm layer. Since the source of the PV is the net wind curl $\Delta\tau$ over the warm water and the primary sink is the eddy flux across the subtropical front (Harrison 1981), the PV budget states

$$K\left(P-\frac{f_0}{H_m}\right)=-\frac{\Delta\tau}{\rho_0 H_m}, \tag{7}$$

where P is the homogenized PV we seek to determine, f_0, the Coriolis parameter at the subtropical front (30°N), $H_m \approx 200\ \mathrm{m}$ is the mixed-layer depth, and $\Delta\tau = 0.28\ \mathrm{N}\cdot\mathrm{m}^{-2}$ is the zonal wind range across the subtropics. Rearranging Eq. (7), we obtain

$$P=\frac{f_0}{H_m}\lambda, \tag{8}$$

where

$$\lambda = 1-\frac{\Delta\tau}{\rho_0 f_0 K}, \tag{9}$$

thus specifies the homogenized PV. In addition, let H denotes the maximum thermocline depth just south of the narrow GSE, it is then given by

$$H=\frac{f_0}{P}=\frac{H_m}{\lambda}. \tag{10}$$

Based on K estimated earlier, λ has the range $[0.2-0.4]$. So H has the range $[500-1000]\ \mathrm{m}$, and the corresponding PV is $[0.73-1.45]\times 10^{-7}\ \mathrm{m}^{-1}\cdot\mathrm{s}^{-1}$ (shown by the gray region in Figure 8). The PV value given here is a plausible range, not an exact value, because we diagnose it based on the asymptotic limit of fully homogenized PV, and then there are uncertainties in other parameters in the calculation of the PV values, including the density difference across the front. In Figure 8, we plot the columnar PV averaged between 10°E and 30°E to examine its variation with the latitude in the subtropical gyre. We have considered the latitude band between 10°N marking the southern extent of the subtropics and the outcrop region, which is defined by the thermocline reaches the base of the mixed layer within which the isopycnals are largely vertical. Instead of aligning with the maximum westerly, the outcrop latitude is shifted southward about 5 degrees from D1 to D32, which can be attributed to heightened eddy mixing (Lévy et al. 2010). In D1, the PV increases strongly with the latitude, spanning a range of about $1.7 \times 10^{-7}\ \mathrm{m}^{-1} \cdot \mathrm{s}^{-1}$ in the subtropics. This range is progressively reduced by increasing resolution, and in D32, it spans only about $0.4 \times 10^{-7}\ \mathrm{m}^{-1} \cdot \mathrm{s}^{-1}$, or only approximately 25% of the non-eddy case. This provides a quantitative statement of the PV homogenization by the eddy mixing. In support of the range of the homogenized PV diagnosed earlier, the PV profile of D32 falls within this range (shaded).

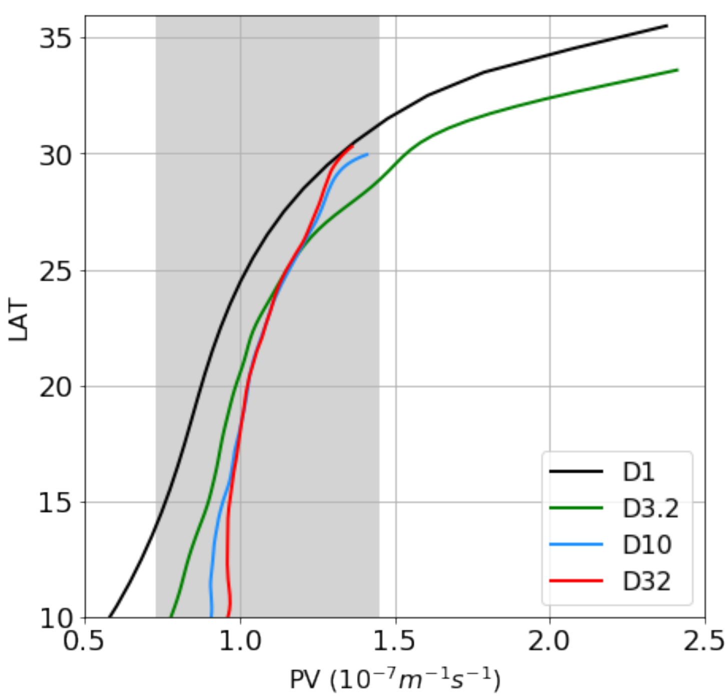

Figure 8. The columnar PV, zonally averaged between 10°E and 30°E, and plotted against latitude spanning the subtropics. These four lines terminate at the outcrop latitude, and the gray region indicates the range of the homogenized PV calculated from the PV budget.

5 PV mixing and Sverdrup balance

Eq. (3) indicates that the large-scale circulation of the upper ocean is primarily modulated by two regimes: PV mixing versus Sverdrup balance. Having discussed the role of eddy mixing in the PV distribution, we focus in this section the relative contributions of these two regimes to the subtropical circulation.

As a zeroth-order theory of the wind-driven motion, the Sverdrup balance is based on the laminar dynamics hence is not expected to apply where the eddy mixing of PV is strong. The two-layer quasi-geostrophic model of Holland (1980) has examined the applicability of the Sverdrup dynamics in a two-gyre basin containing energetic eddies and showed that the Sverdrup balance holds only over a small fraction of the basin (his Figure 3). Observational analysis incorporating Argo floats (Gray and Riser 2014) suggests that the Sverdrup dynamics may account for the meridional transports in the tropics and subtropics, but fails in higher latitudes and boundary regions due to the effects of barotropic flow, nonlinear dynamical processes, and topography. Few studies have examined the effect of the eddy mixing on the Sverdrup relationship in the interior -- a significant gap we seek to fill in this study.

To quantify the effects of eddy mixing on the Sverdrup balance, we define from Eq. (5) the deviation from the classical Sverdrup balance

$$\Delta = -\frac{\tau_y^x}{\rho_0} - \beta h v. \tag{11}$$

We then calculate the ratio

$$\varepsilon = \frac{|\Delta|}{|\tau_y^x/\rho_0|}, \tag{12}$$

which can be interpreted as the percentage within which the Sverdrup balance holds. The closer to zero ε is, to a greater degree the Sverdrup balance holds. Following Holland (1980), we set $\varepsilon <$

0.2 as the spatial domain where the Sverdrup balance approximately holds, which we shall refer for convenience as the Sverdrup domain. This domain is shown by shaded regions in Figure 9, which is overlaid with the thermocline depth in red contours. For the coarse-grid experiment (D1), the Sverdrup domain covers the whole subtropics except near the western boundary layer where the inertial-viscous balance dominates (Munk 1950; Pedlosky 1987). For the eddy-permitting experiment (D3.2), the Sverdrup domain has shrunk considerably to limited regions in the interior and near the eastern boundary. This trend continues for the eddy-resolving experiment (D10) with much enhanced eddy mixing, and for the fine-grid experiment (D32), additional mixing mechanisms, such as the chaotic stirring, has further reduced the Sverdrup domain to a few isolated patches. Quantitatively, from D1 to D32, the Sverdrup domain in the subtropics has shrunk by more than 60%, which provides another quantitative statement of the PV-mixing effect. Surface eddy diffusivities derived from satellite altimetry show that the horizontal mixing in the subtropical interior is much weaker than where there is strong current (Abernathey et al. 2013), our results suggest however that the eddy effects on the PV cannot be neglected in the quieter subtropical interior.

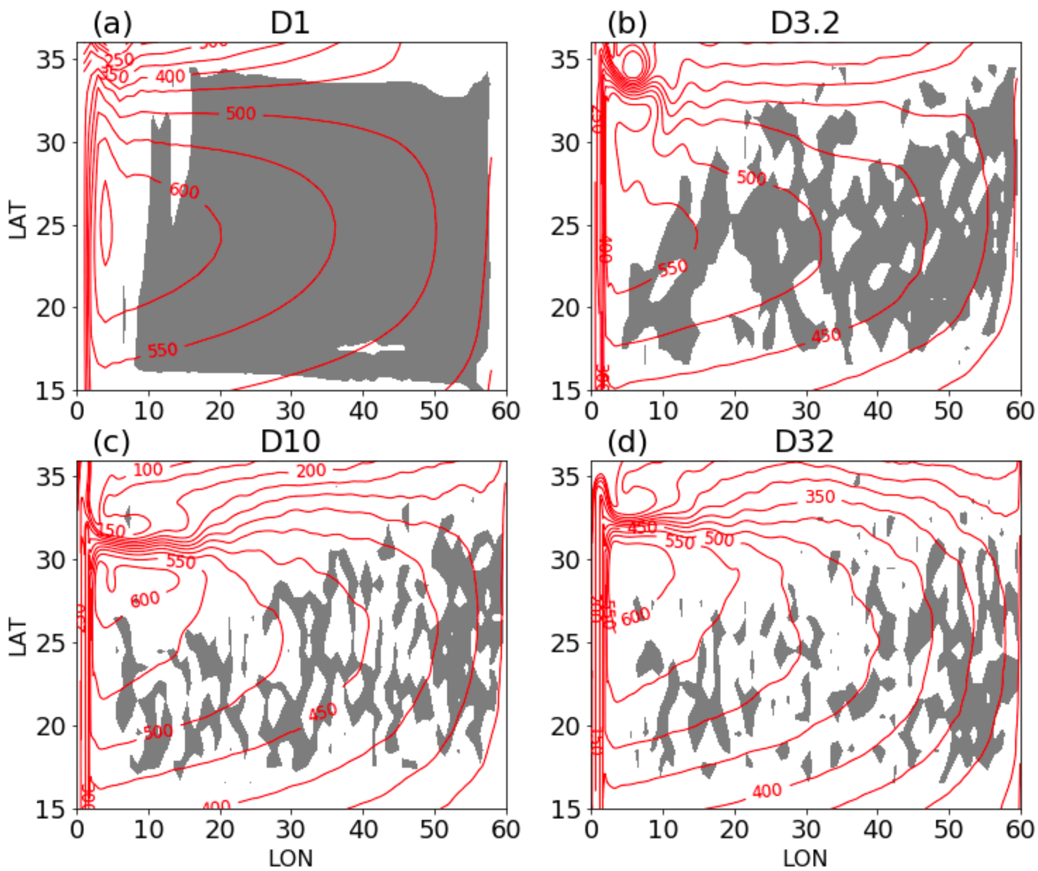

Figure 9. Sverdrup domain (shaded) with the depth of the 26.5 isopycnal overlaid in red contours. The Sverdrup domain is defined by ε (Eq. 12) being smaller than 0.2.

Since the general ocean circulation has largely converged from 1/10° to 1/32° and given the inordinate computational resources required of 1/32° runs, it suffices to use the 1/10° experiment to examine the solution sensitivity to the varying wind profile. In Figure 10, we compare the thermocline depth from the coarse-grid (D1) and eddy-resolving (D10) runs with the analytical solutions from the Sverdrup and PV mixing regimes, respectively. For the numerical solutions, three wind profiles are used to assess their sensitivity. In Figure 10(a), the analytical Sverdrup solution is calculated from (Huang 2010),

$$h^2 = h_e^2 + \frac{2f^2}{g'\rho_0\beta}\left(\frac{\tau^x}{f}\right)_y L, \tag{13}$$

where the thermocline depth at the eastern boundary h_e is set to $400\ \mathrm{m}$, reduced gravity $g' = 0.02\ \mathrm{m \cdot s^{-2}}$, L is the distance from the eastern boundary. It is seen that the coarse-grid solutions (solid lines) indeed trace closely the analytical curve (dashed line) to fall within the Sverdrup regime. The latitude of the maximum thermocline depth aligns roughly with that of the maximum wind stress curl and the numerical solutions shift with the different winds, both as predicted from Eq. (13).

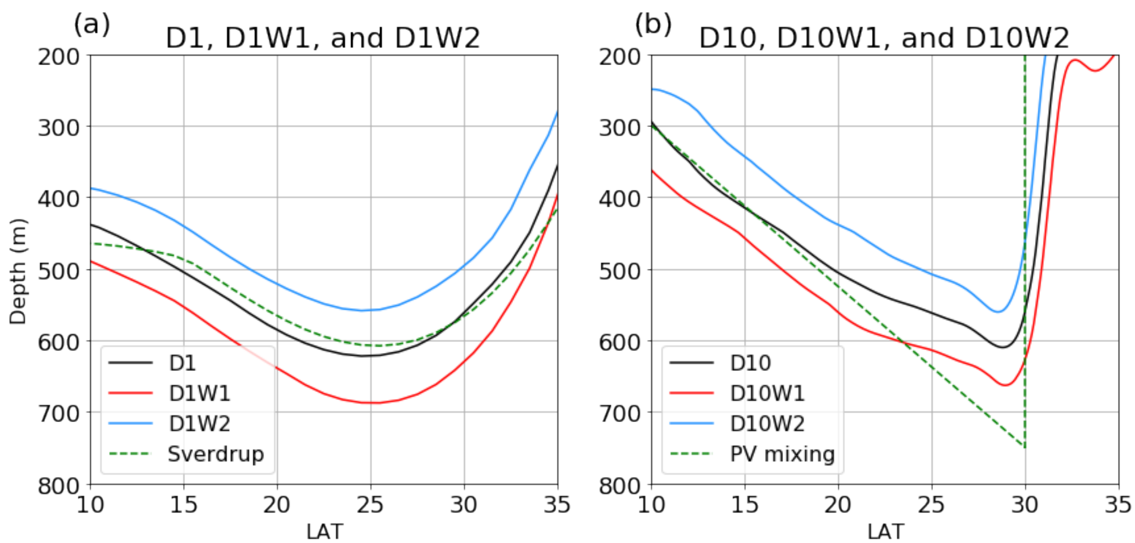

Figure 10. Comparison of the thermocline depth along 12°E between the numerical and analytical solutions. (a) The coarse-grid (1°) numerical solutions using different wind profiles (colored lines) and the analytical Sverdrup solution (dashed line); (b) Same as (a) but the numerical solutions are from eddy-resolving (1/10°) calculations and the analytical solution is based on the homogenized PV.

In Figure 10(b), the analytical solution of the homogenized PV with its medium value (as estimated in Section 4) is used here for the theoretical curve. Since the relative vorticity is negligible in the subtropical interior, the homogenized PV implies that the thermocline deepens linearly with the latitude before it shoals abruptly across the subtropical front. The eddy-resolving solutions are seen to compare closely with the analytical solution, in support of the PV homogenization. Varying wind also shifts the numerical solution in accordance with the theoretical prediction (Eq. 10). While there remains some difference between the numerical and analytical solutions it is patently clear that the PV mixing regime provides a better explanation of the eddy-resolving solutions than the Sverdrup regime.

6 Summary and discussion

Classic wind-driven theories based on the Sverdrup balance have difficulties in explaining some features of the observed circulation. This is because these theories mostly do not consider the eddy mixing, which tends to homogenize the macroscopic PV to abridge the Sverdrup balance. In its application to the atmosphere, Ou (2013) shows that the PV homogenization may reproduce the prevailing wind, which thus may serve as a governing principle of the general atmospheric circulation. The present study aims to assess the role of eddy mixing of the PV in the general ocean circulation. Although PV homogenization in the subtropical ocean has been discerned by observations and numerical models (McDowell 1982; Cox 1985), we attempt to provide a quantitative assessment of the regime from numerical experiments.

We consider an idealized ocean basin in the Northern Hemisphere and carry out a series of numerical experiments using the MITgcm with varying horizontal grid spacings and wind forcings. To assess the effect of eddy mixing on the upper-ocean circulation, numerical calculations using four grid spacings of 1°, 1/3.2°, 1/10°, and 1/32° are carried out. With increasing resolution from the coarse-grid to the eddy-resolving runs, the teeming eddies emerge to qualitatively alter the macroscopic circulation. For the eddy resolving runs of 1/10°, the EKE attains the same order of magnitude as the observed one, and for the fine-grid runs of 1/32°, the maximum EKE exceeds $2000\ \mathrm{cm}^2 \cdot \mathrm{s}^{-2}$ hence comparable to that observed. Such fine-grid resolution has not been widely attempted in simulating the general ocean circulation, but is seen to be needed to capture adequately the eddy-mixing effect. In the coarse-grid case, the structure of the thermocline is as expected from the Sverdrup dynamics with its maximum depth located in the subtropical interior. With increasing resolution, this maximum depth is seen to migrate toward the subtropical front. Particularly, the eddy-resolving (1/10°) and fine-grid (1/32°) experiments show a thermocline that deepens linearly with latitude until it shoals abruptly across the subtropical front, which is consistent with its observed structure (Qiu et al. 2010).

Although several studies (Cox 1985; Henning and Vallis 2004; Lévy et al. 2010) have discerned the changing subtropical circulation when eddies are resolved, our principal innovation is to provide a quantitative assessment of the eddy-mixing regime by comparing the numerical and analytical solutions. Our numerical solutions show that eddy mixing is quite effective in homogenizing the PV in the subtropical gyre, reducing its spatial range by about 75% when the grid spacing decreases from 1° to 1/32°. We also find that the Sverdrup domain is relegated to isolated patches in the fine-grid (1/32°) experiments, with its area reduced by about 60% from the coarse-grid runs. In addition, sensitivity experiments show that the thermocline depth is modulated by wind-curl, as predicted by both Sverdrup and homogenized-PV regimes. In eddy-resolving cases, the observed thermocline structure is well reproduced by the homogenized PV regime, the latter thus provides a better explanation of the subtropical gyre than the Sverdrup dynamics.

Lastly, we need to acknowledge the limitations of this study. First, to simplify the question and compare with the classic Sverdrup theory, we have not considered the vertical structure of the circulation and vertical eddy flux (e.g. Zhai and Marshall 2013) in the discussions of PV homogenization. Second, in our budget calculation, we have neglected the PV sink at the boundaries due to the viscous drag (the sole sink in the Sverdrup regime), which would modify the value of the homogenized PV. Third, the fully PV homogenization in the subtropical gyre is obtained in the hypothesis of infinitely strong eddy mixing, which is the gap between the PV mixing theory and the observations.

It should be noted that this study is not intended to replace these theories based on the Sverdrup dynamics, but merely to present a novel perspective to explain the complicated general ocean circulation. In spite of these limitations of PV mixing regime, our conclusions from this study remain clear: the effects of eddy mixing are essential and must be included in the theory of the general ocean circulation.

Acknowledgments

T. Liu, X. Liu, and D. Chen are supported by the National Natural Science Foundation of China (41730535) and the China Postdoctoral Science Foundation (2020M681968). H. W. Ou's contribution is not supported by any external grants. All computations and analysis in this study are implemented on the Tianhe-2 supercomputer. The dataset of World Ocean Atlas 2013 is available at https://www.nodc.noaa.gov/OC5/woa13/.

References

Abernathey, R. P., & Marshall, J. (2013). Global surface eddy diffusivities derived from satellite altimetry. *Journal of Geophysical Research: Oceans*, *118*(2), 901-916. https://doi.org/10.1002/jgrc.20066.

Brown, M. G., & Smith, K. B. (1991). Ocean stirring and chaotic low-order dynamics. *Physics of Fluids A: Fluid Dynamics, 3*(5), 1186-1192. https://doi.org/10.1063/1.858047.

Bryan, F. O., Hecht, M. W., & Smith, R. D. (2007). Resolution convergence and sensitivity studies with North Atlantic circulation models. Part I: The western boundary current system. *Ocean Modelling, 16*(3-4), 141-159. https://doi.org/10.1016/j.ocemod.2006.08.005.

Charney, J. (1955). The use of the primitive equations of motion in numerical prediction. *Tellus, 7*(1), 22-26. https://doi.org/10.1111/j.2153-3490.1955.tb01138.x.

Chassignet, E. P., & Xu, X. (2017). Impact of horizontal resolution (1/12 to 1/50) on Gulf Stream separation, penetration, and variability. *Journal of Physical Oceanography, 47*(8), 1999-2021.

Cox, M. D. (1985). An eddy resolving numerical model of the ventilated thermocline. *Journal of Physical Oceanography, 15*(10), 1312-1324. https://doi.org/10.1175/1520-0485(1985)015<1312:AERNMO>2.0.CO;2.

Fofonoff, N. P. (1954). Steady flow in a frictionless homogeneous ocean. *Journal of Marine Research, 13*, 254-262.

Fox-Kemper, B., & Menemenlis, D. (2008). Can large eddy simulation techniques improve mesoscale rich ocean models. *Ocean modeling in an eddying regime, 177*, 319-337. https://doi.org/10.1029/177GM19.

Fu, L. L., Chelton, D. B., Le Traon, P. Y., & Morrow, R. (2010). Eddy dynamics from satellite altimetry. *Oceanography, 23*(4), 14-25. https://doi.org/10.5670/oceanog.2010.02.

Gray, A. R., & Riser, S. C. (2014). A global analysis of Sverdrup balance using absolute geostrophic velocities from Argo. *Journal of Physical Oceanography, 44*(4), 1213-1229. https://doi.org/10.1175/JPO-D-12-0206.1.

Hall, M. M. (1989). Velocity and transport structure of the Kuroshio Extension at 35 N, 152 E. *Journal of Geophysical Research: Oceans, 94*(C10), 14445-14459. https://doi.org/10.1029/JC094iC10p14445.

Harrison, D. E. (1981). Eddy lateral vorticity transport and the equilibrium of the North Atlantic subtropical gyre. *Journal of Physical Oceanography, 11*(8), 1154-1159. https://doi.org/10.1175/1520-0485(1981)011<1154:ELVTAT>2.0.CO;2.

Henning, C. C., & Vallis, G. K. (2004). The effects of mesoscale eddies on the main subtropical thermocline. *Journal of physical oceanography, 34*(11), 2428-2443. https://doi.org/10.1175/JPO2639.1.

Hogg, A. M., & Gayen, B. (2020). Ocean gyres driven by surface buoyancy forcing. *Geophysical Research Letters, 47*(16), e2020GL088539. https://doi.org/10.1029/2020GL088539.

Holland, W. R., Keffer, T., & Rhines, P. B. (1984). Dynamics of the oceanic general circulation: the potential vorticity field. *Nature, 308*(5961), 698-705. https://doi.org/10.1038/308698a0.

Holland, W. R., & Rhines, P. B. (1980). An example of eddy-induced ocean circulation. *Journal of Physical Oceanography, 10*(7), 1010-1031. https://doi.org/10.1175/1520-0485(1980)010<1010:AEOEIO>2.0.CO;2.

Huang, R. X. (1988). On boundary value problems of the ideal-fluid thermocline. *Journal of physical oceanography, 18*(4), 619-641. https://doi.org/10.1175/1520-0485(1988)018<0619:OBVPOT>2.0.CO;2.

Huang, R. X. (2010). Ocean circulation: wind-driven and thermohaline processes. *Cambridge University Press.*

Hurlburt, H. E., & Hogan, P. J. (2000). Impact of 1/8 to 1/64 resolution on Gulf Stream model–data comparisons in basin-scale subtropical Atlantic Ocean models. *Dynamics of Atmospheres and Oceans, 32*(3-4), 283-329. https://doi.org/10.1016/S0377-0265(00)00050-6.

Keffer, T. (1985). The ventilation of the world's oceans: Maps of the potential vorticity field. *Journal of physical oceanography, 15*(5), 509-523. https://doi.org/10.1175/1520-0485(1985)015<0509:TVOTWO>2.0.CO;2.

Lévy, M., Klein, P., Tréguier, A. M., Iovino, D., Madec, G., Masson, S., & Takahashi, K. (2010). Modifications of gyre circulation by sub-mesoscale physics. *Ocean Modelling, 34*(1-2), 1-15. https://doi.org/10.1016/j.ocemod.2010.04.001.

Liu, T., Abernathey, R., Sinha, A., & Chen, D. (2019). Quantifying Eulerian Eddy Leakiness in an Idealized Model. *Journal of Geophysical Research: Oceans, 124*(12), 8869-8886. https://doi.org/10.1029/2019JC015576.

Luyten, J. R., Pedlosky, J., & Stommel, H. (1983). The ventilated thermocline. *Journal of Physical Oceanography, 13*(2), 292-309. https://doi.org/10.1175/1520-0485(1983)013<0292:TVT>2.0.CO;2.

McCartney, M. S., & Talley, L. D. (1982). The subpolar mode water of the North Atlantic Ocean. *Journal of Physical Oceanography, 12*(11), 1169-1188. https://doi.org/10.1175/1520-0485(1982)012<1169:TSMWOT>2.0.CO;2.

McDowell, S., Rhines, P., & Keffer, T. (1982). North Atlantic potential vorticity and its relation to the general circulation. *Journal of Physical Oceanography, 12*(12), 1417-1436. https://doi.org/10.1175/1520-0485(1982)012<1417:NAPVAI>2.0.CO;2.

Marshall, J., Adcroft, A., Hill, C., Perelman, L., & Heisey, C. (1997). A finite-volume, incompressible Navier Stokes model for studies of the ocean on parallel computers. *Journal of Geophysical Research: Oceans, 102*(C3), 5753-5766. https://doi.org/10.1029/96JC02775.

Marshall, J., Jones, H., Karsten, R., & Wardle, R. (2002). Can eddies set ocean stratification?. *Journal of physical oceanography, 32*(1), 26-38. https://doi.org/10.1175/1520-0485(2002)032<0026:CESOS>2.0.CO;2.

Marshall, J., & Nurser, G. (1986). Steady, free circulation in a stratified quasi-geostrophic ocean. *Journal of physical oceanography, 16*(11), 1799-1813. https://doi.org/10.1175/1520-0485(1986)016<1799:SFCIAS>2.0.CO;2.

Munk, W. H. (1950). On the wind-driven ocean circulation. *Journal of Atmospheric Sciences, 7*(2), 80-93. https://doi.org/10.1175/1520-0469(1950)007<0080:OTWDOC>2.0.CO;2.

Munk, W. (2002). The evolution of physical oceanography in the last hundred years. *Oceanography, 15*(1):135–141. https://doi.org/10.5670/oceanog.2002.45.

Nakamura, M., & Kagimoto, T. (2006). Potential vorticity and eddy potential enstrophy in the North Atlantic Ocean simulated by a global eddy-resolving model. *Dynamics of atmospheres and oceans, 41*(1), 28-59. https://doi.org/10.1016/j.dynatmoce.2005.10.002.

Ou, H. W. (2013). Upper-bound general circulation of coupled ocean–atmosphere: Part 1. Atmosphere. *Dynamics of atmospheres and oceans, 64*, 10-26. https://doi.org/10.1016/j.dynatmoce.2013.09.001.

Ou, H. W. (2018). Thermohaline circulation: a missing equation and its climate-change implications. *Climate dynamics, 50*(1), 641-653. https://doi.org/10.1007/s00382-017-3632-y.

Pedlosky, J. (1987). Geophysical fluid dynamics (Vol. 710). *New York: springer*. https://doi.org/10.1007/978-1-4612-4650-3.

Qiu, B., & Chen, S. (2010). Interannual variability of the North Pacific Subtropical Countercurrent and its associated mesoscale eddy field. *Journal of Physical Oceanography, 40*(1), 213-225. https://doi.org/10.1175/2009JPO4285.1.

Renault, L., McWilliams, J. C., & Masson, S. (2017). Satellite observations of imprint of oceanic current on wind stress by air-sea coupling. *Scientific reports, 7*(1), 1-7. https://doi.org/10.1038/s41598-017-17939-1.

Rhines, P. B., & Young, W. R. (1982). Hornogenization of potential vorticity in planetary gyres. *Journal of Fluid Mechanics, 122*, 347-367. https://doi.org/10.1017/S0022112082002250.

Rio, M. H., Guinehut, S., & Larnicol, G. (2011). New CNES-CLS09 global mean dynamic topography computed from the combination of GRACE data, altimetry, and in situ measurements. *Journal of Geophysical Research: Oceans, 116*(C7). https://doi.org/10.1029/2010JC006505.

Rocha, C. B., Gille, S. T., Chereskin, T. K., & Menemenlis, D. (2016). Seasonality of submesoscale dynamics in the Kuroshio Extension. *Geophysical Research Letters, 43*(21), 11-304. https://doi.org/10.1002/2016GL071349.

Smith, R. D., Maltrud, M. E., Bryan, F. O., & Hecht, M. W. (2000). Numerical simulation of the North Atlantic Ocean at 1/10. *Journal of Physical oceanography, 30*(7), 1532-1561. https://doi.org/10.1175/1520-0485(2000)030<1532:NSOTNA>2.0.CO;2.

Stommel, H. (1948). The westward intensification of wind-driven ocean currents. *Eos, Transactions American Geophysical Union, 29*(2), 202-206. https://doi.org/10.1029/TR029i002p00202.

Stommel, H. M. (1965). The Gulf Stream: a physical and dynamical description. *University of California Press*.

Su, Z., Wang, J., Klein, P., Thompson, A. F., & Menemenlis, D. (2018). Ocean submesoscales as a key component of the global heat budget. *Nature communications, 9*(1), 1-8. https://doi.org/10.1038/s41467-018-02983-w.

Sverdrup, H. U. (1947). Wind-driven currents in a baroclinic ocean; with application to the equatorial currents of the eastern Pacific. *Proceedings of the National Academy of Sciences of the United States of America, 33*(11), 318. https://doi.org 10.1073/pnas.33.11.318.

Talley, L. D. (1988). Potential vorticity distribution in the North Pacific. *Journal of Physical Oceanography, 18*(1), 89-106. https://doi.org/10.1175/1520-0485(1988)018<0089:PVDITN>2.0.CO;2.

Toole, J. M., Millard, R. C., Wang, Z., & Pu, S. (1990). Observations of the Pacific North Equatorial Current bifurcation at the Philippine coast. *Journal of Physical Oceanography, 20*(2), 307-318. https://doi.org/10.1175/1520-0485(1990)020<0307:OOTPNE>2.0.CO;2.

Welander, P. (1968). Wind-driven circulation in one-and two-layer oceans of variable depth. *Tellus, 20*(1), 1-16. https://doi.org/10.1111/j.2153-3490.1968.tb00347.x.

Wenegrat, J. O., Thomas, L. N., Gula, J., & McWilliams, J. C. (2018). Effects of the submesoscale on the potential vorticity budget of ocean mode waters. *Journal of Physical Oceanography, 48*(9), 2141-2165. https://doi.org/10.1175/JPO-D-17-0219.1.

Young, W. R. (1987). Baroclinic theories of the wind driven circulation. *General circulation of the Ocean*, 134-201. https://doi.org/10.1007/978-1-4612-4636-7_4.

Zhai, X., & Marshall, D. P. (2013). Vertical eddy energy fluxes in the North Atlantic subtropical and subpolar gyres. *Journal of physical oceanography, 43*(1), 95-103. https://doi.org/10.1175/JPO-D-12-021.1.